RELIABILITY TESTING AND IMPROVEMENT OF POLYMER HINGE-BASED MEMS SCANNING MIRRORS

A Thesis

by

HASAN MD. RAFSANJANI

Submitted to the Office of Graduate and Professional Studies of
Texas A&M University
in partial fulfillment of the requirements for the degree of

MASTER OF SCIENCE

Chair of Committee,	Jun Zou
Committee Members,	Xiaoning Qian
	Sheng-Jen Hsieh
	Paotai Lin
Head of Department,	Miroslav M. Begovic

August 2018

Major Subject: Electrical Engineering

Copyright 2018 Hasan Md. Rafsanjani

ABSTRACT

Ultrasound and photoacoustic imaging techniques can benefit greatly combined with MEMS scanning mirror technology. Such mirrors can be designed with small enough form factors to fit into handheld imaging probes and the study presented in this thesis goes into (1) analyzing the performance of such a single-axis scanning mirror, (2) improving its design to function more robustly at higher scanning angles, (3) allow for precise monitoring and control of the angle using magnetic sensor.

The scanning mirror consists of an aluminum deposited silicon mirror plate on top of a laser-cut flexible polymer double hinge structure and two permanent magnets, which allow for single-axis movement through electromagnetic actuation. This mirror's operation was tested to verify its reliability. Through the tests, it was determined that the device could reliably operate at ±3° scanning angles without any degradation in performance, but at ±6° showed a steady decline in performance.

Following these results, the mirror design was modified by doubling the length of the polymer hinges to generate twice the scanning angle. The redesigned mirror's operation was tested ±6° scanning angle and proven to no longer go through performance degradation. The resonant frequency under water of the new mirror was also boosted by replacing the rectangular mirror plate with an elliptical one, fabricated using reactive ion etch.

A linear-Hall effect sensor was also later added to the device and calibrated accordingly to allow for more precise monitoring of the scanning angle and hence, further improve the reliability of our final mirror device package.

DEDICATION

To my family, mentors and friends

ACKNOWLEDGEMENTS

I would like to first and foremost express my heartfelt gratitude to my research advisor and committee chair, Dr. Zou, for his invaluable guidance throughout every stage of my research work and education over the past two years. I would also like to sincerely thank my committee members Dr. Qian, Dr. Lin and Dr. Hsieh, for agreeing to oversee my thesis work and for their continued patience with me.

Thanks also to my research group colleagues Song, Zhiyu, Xiaoyu, Cheng, Arif and Young whose instructions and training helped me get a running start to my research work and progress smoothly to the very end. The Texas A&M AggieFab and ECE staff have also all been wonderful and accommodating over my program here and I am deeply appreciative of their assistance.

Finally, I would like to thank my family for their endless love, encouragement and support.

CONTRIBUTORS AND FUNDING SOURCES

This work was supervised by a thesis committee consisting of Professor Jun Zou and Professors Xiaoning Qian and Paotai Lin of the Department of Electrical and Computer Engineering, and Professor Sheng-Jen Hsieh of the Department of Engineering Technology and Industrial Distribution.

All work for the thesis was completed by the student, under the advisement of Professor Jun Zou of the Department of Electrical and Computer Engineering.

There are no outside funding contributions to acknowledge related to the research and compilation of this document.

TABLE OF CONTENTS

Page

ABSTRACT ii

DEDICATION iv

ACKNOWLEDGEMENTS v

CONTRIBUTORS AND FUNDING SOURCES vi

TABLE OF CONTENTS vii

LIST OF FIGURES ix

LIST OF TABLES xi

1. INTRODUCTION 1

    1.1 Background 1
    1.2 Summary of work 2

2. RELIABILITY TESTING OF POLYMER HINGE-BASED SCANNING MIRROR 4

    2.1 Mirror design and operation summary 4
    2.2 Characterization of scanning mirror device 4
    2.3 Reliability testing of mirror in water, continuous run 8
    2.4 Reliability testing of mirror in water, cycles 10
    2.5 Reliability testing of mirror in air, cycles 13
    2.6 Reliability testing of mirror in water, large angle, cycles 15
    2.7 Conclusion 17

3. DESIGN AND FABRICATION OF NEW MIRROR DEVICE AND FURTHER RELIABILITY TESTING 18

    3.1 Improvements to mirror device design and fabrication overview 18
    3.2 Characterization and testing of new mirror device 20
    3.3 Fabrication of elliptical mirror plate 21
    3.4 Characterization and reliability testing of device with elliptical mirror plate 22

Page

3.5 Conclusion 26

4. IMPLEMENTATION OF SCANNING ANGLE MEASUREMENT SYSTEM 27

4.1 Introduction 27
4.2 Magnetic field simulation and Hall sensor specifications 27
4.3 Hall sensor characterization 29
4.4 3D printing of new holder and device assembly 31
4.5 Calibration and testing of Hall sensor scanning angle monitoring 33
4.6 Conclusion 34

5. CONCLUSION AND FUTURE WORKS 36

REFERENCES 39

LIST OF FIGURES

Page

Figure 2.1 (a) Schematic side view of mirror and (b) 3D model of mirror 4

Figure 2.2 Laser tracing setup 5

Figure 2.3 Device characterization in air, signal frequency vs. scanning angle 6

Figure 2.4 Device characterization in air, driving current vs. scanning angle 6

Figure 2.5 Device characterization in water, signal frequency vs. scanning angle.. 7

Figure 2.6 Device characterization in water, driving current vs. scanning angle 7

Figure 2.7 Reliability testing data, cycles 8

Figure 2.8 Resonant frequency vs. driving current shifts 9

Figure 2.9 Reliability testing data in water, continuous run 11

Figure 2.10 Reliability testing resonant frequency data in water, continuous run... 13

Figure 2.11 Reliability testing data in air, cycles 14

Figure 2.12 Reliability testing resonant frequency data in air, cycles 14

Figure 2.13 Reliability testing data in water, large angle, cycles..... 15

Figure 2.14 Reliability testing resonant frequency data, large angle, cycles 16

Figure 3.1 (a) Previous hinge design and (b) new hinge design 19

Figure 3.2 Test data in water, new device 20

Figure 3.3 (a) Photomask layout for elliptical mirrors and (b) etched out mirror plates..... 22

Figure 3.4 3D Model of new mirror 23

Figure 3.5 Reliability test data in water, new device 24

Page

Figure 3.6 Reliability test resonant frequency data in water, new device 25

Figure 4.1 FEMM simulation of device configuration permanent magnets 28

Figure 4.2 Region of interest for Hall sensor placement..... 28

Figure 4.3 (a) Honeywell SS49E Hall sensor and (b) its response provided in specification sheet 29

Figure 4.4 Experimental setup for Hall sensor characterization 30

Figure 4.5 Hall sensor characterization, output voltage vs. separation..... 30

Figure 4.6 Hall sensor characterization, sensitivity vs. separation 31

Figure 4.7 (a) 3D Model of new holder and (b) 3D printed new holder..... 32

Figure 4.8 (a) Assembled device package and (b) top view 33

Figure 4.9 Hall sensor data from angle monitoring calibration and test..... 34

LIST OF TABLES

Page

Table 1 Characterization results of new mirror device 20

Table 2 Characterization results of new mirror device with elliptical mirror plate 23

1. INTRODUCTION

1.1 Background

Ultrasound and photoacoustic imaging technologies are used in a variety of non-destructive and in-vivo biomedical imaging applications. Traditional ultrasound imaging works by sending pulses of sound waves in the 1-5 megahertz range using a transducer, and by picking up the waves reflected back from different boundaries of the biological target, an image of the internal structures can be generated. Photoacoustic imaging works by utilizing the photoacoustic effect which results from the absorption of electromagnetic waves such as pulsed laser or radio-frequency waves to induce vibrations in the target biological sample and generate acoustic waves in the ultrasound range, which is then picked up through receivers to construct an image.

Such imaging techniques when combined with the precision of scanning mirror devices can be used to obtain high spatial resolution microscopic images of deep tissues, internal organs, vascular morphology and gather important physiological and biochemical information such as blood oxygenation levels to detection of tumors and cancer [1-2]. Microelectromechanical systems (MEMS) mirrors allow for precision steering of the involved optical and acoustic waves and fast scanning of the target samples.

However, conventional silicon-based MEMS mirrors are ineffective in such microscopic imaging applications since a liquid medium is necessary for efficient transmission of ultrasound waves. Silicon structures are often too fragile in liquid environments and are prone to breakage and degradation from turbulence, excessive

damping and surface tension forces as compared to operation in air. MEMS mirrors that can operate readily in water as in air is crucial in such imaging systems which signals the need for an innovative mirror design utilizing materials outside silicon to form the actuating parts.

1.2 Summary of work

In chapter 2 of this thesis, analysis and reliability testing of a single-axis polymer hinge-based water-immersible MEMS scanning mirror design is carried out. Extensive testing is done using this mirror in both air and water medium and at two different scanning angles in water. The results of these tests concluded that, at the higher scanning angle, a degradation in performance occurs in the mirror with continued operation.

Chapter 3 goes into the process of improving the mirror design to tackle this degradation issue and the fabrication of the new mirror. The length of the polymer hinges is doubled in the new design and the rectangular mirror plate is changed out for an elliptical one to reduce the fluid damping resistance during operation. This new mirror is then characterized in air and water and then afterwards run through the same reliability testing process. The testing results concluded that the performance degradation issue had been solved with the new changes in design.

Chapter 4 details the incorporation of a linear Hall-effect sensor into our mirror device to further improve the reliability and repeatability of its performance. The sensitivity curve of the Hall sensor is first acquired through experimentation and then added to our mirror device. The readings of the Hall sensor are then calibrated to the

respective scanning angle of the mirror, and following that, any change in the scanning angle could be reliably picked up by a corresponding change in the Hall sensor reading, allowing for precise control and monitoring of the angle in our final mirror device.

2. RELIABILITY TESTING OF POLYMER HINGE-BASED SCANNING MIRROR

2.1 Mirror design and operation summary

The schematic design of the single-axis polymer-based scanning mirror is given in Figure 2.1 [3]. The mirror plate is attached atop the biaxially oriented polyethylene teraphtalate (BOPET) hinge structure and is actuated by passing an AC signal through the inductor coil which interacts with the magnetic field produced by the permanent magnet configuration and generates the oscillating motion of the mirror plate.

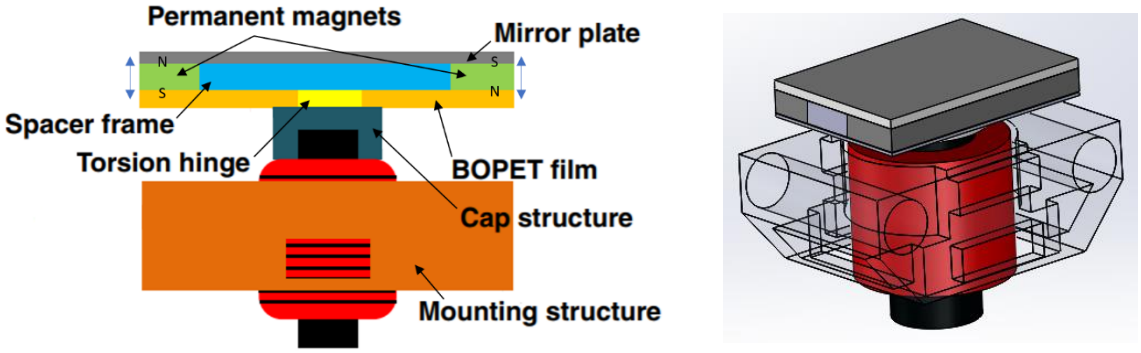

Figure 2.1 (a) Schematic side view of mirror and (b) 3D model of mirror. Modified from [3]

2.2 Characterization of scanning mirror device

The characterization of the mirror was done using a laser-tracing method [3-4]. An acrylic holder piece was taped to a mounting stand first, and the mirror device is set on the acrylic holder piece using screws. The screw holes on the acrylic holder was placed along a 45° line to the horizontal which holds the mirror at the same angle and reflect the

horizontally incident laser beam to bounce off the mirror plate straight down onto the ruler. The distance between the mirror and the ruler on the bottom is 19.5 cm and through trigonometry, the scanning angle of the mirror could be determined by the length of the laser trace incident on the ruler.

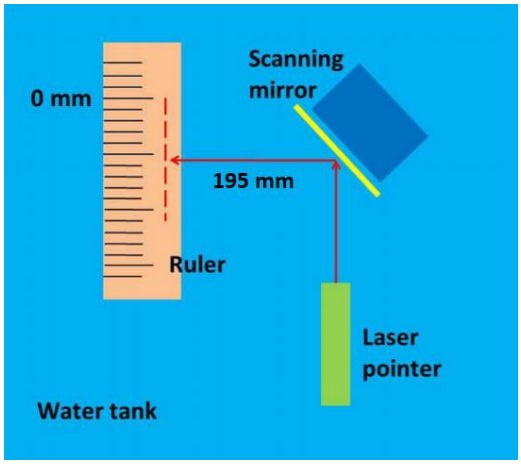

Figure 2.2 Laser tracing setup. Modified from [3]

An AC signal generator was used to generate the driving signal which is passed through the inductor coil, and a parameter analyzer connected in series reads the driving current passing through the coil at the respective signal voltage amplitude. To characterize the performance of the mirror versus the frequency of the driving signal, a driving current of 20 mA was passed through the inductor coil and the frequency of the signal was swept from 50 Hz to 250 Hz. The obtained scanning angle versus the frequency plot is given in Figure 2.3 and from it the resonant frequency of the device was determined to be 218 Hz,

producing a scanning angle of ±8.89°. All angles mentioned hereon are actually half-angles, meaning the device's maximum angular displacement from the center axis.

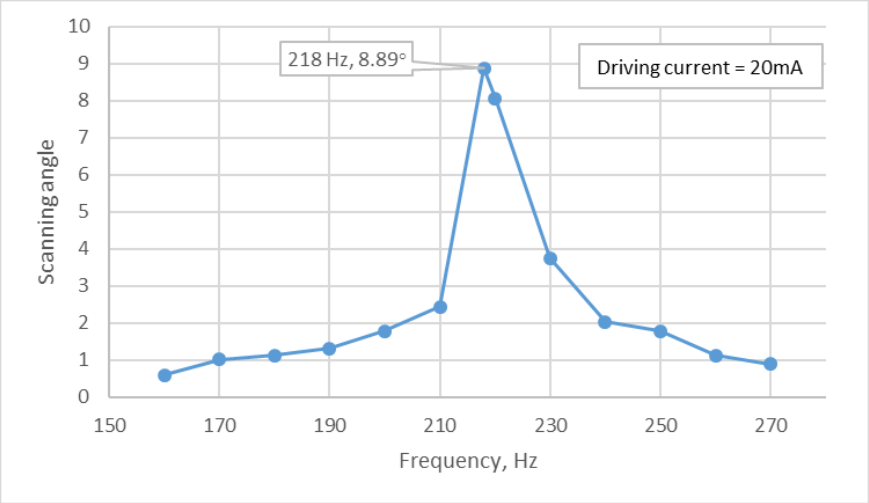

Figure 2.3 Device characterization in air, signal frequency vs. scanning angle

The 218 Hz resonant frequency was then used as our signal frequency in the next experiment to determine the scanning angle produced versus the driving current. The angles of operation of concern for this device are ±3° and ±6° which were attained at 9.45 mA and 14.2 mA, respectively, as could be determined using the plot shown in Figure 2.4. The response also seemed to be fairly linear.

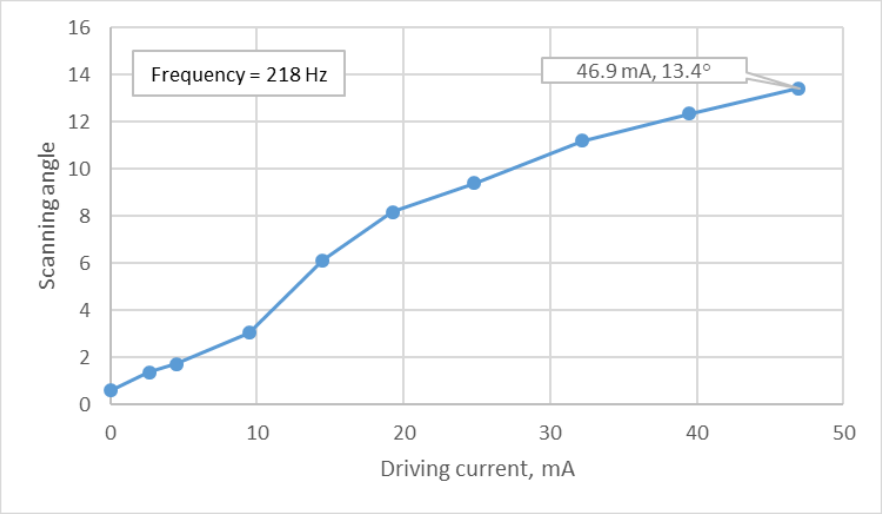

Figure 2.4 Device characterization in air, driving current vs. scanning angle

The same characterization experiment was carried out in water medium, with the mounting stand holding the device placed underwater along with the ruler. The frequency characterization determined the resonant frequency of the device now to be 183 Hz.

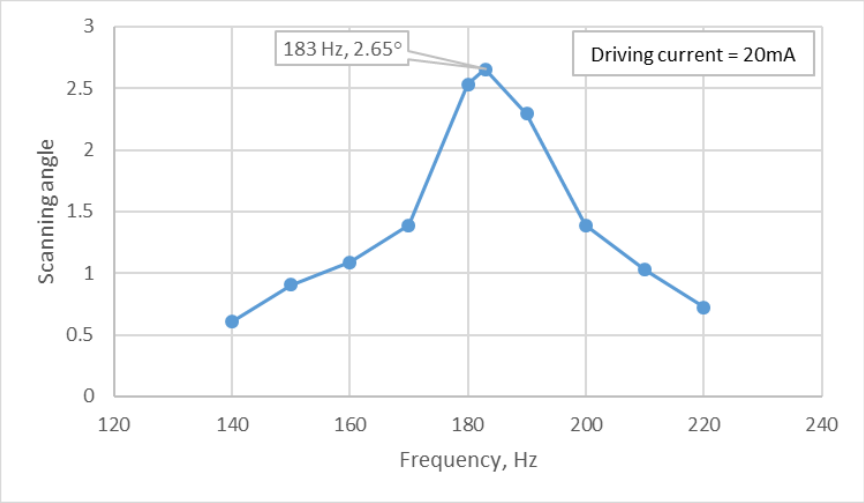

Figure 2.5 Device characterization in water, signal frequency vs. scanning angle

The current characterization provided us values of 22 mA and 60 mA for ±3° and ±6°, respectively. The response was again linear.

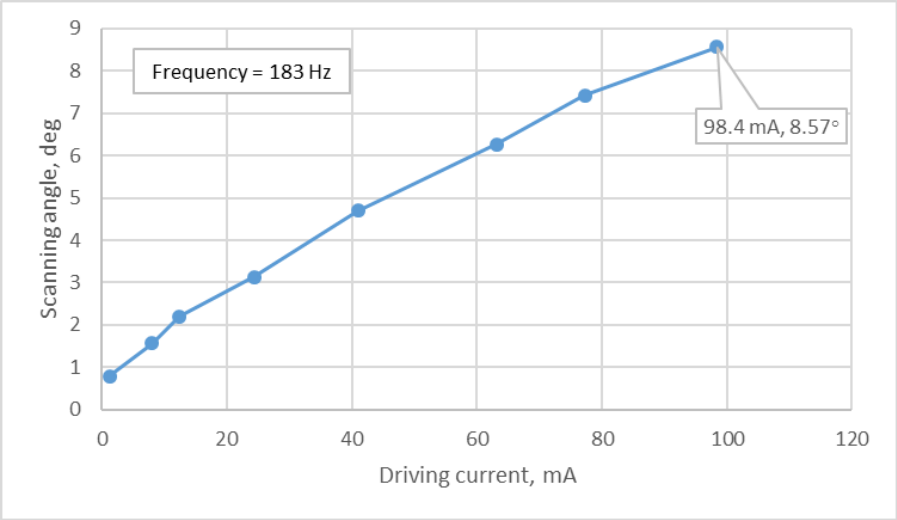

Figure 2.6 Device characterization in water, driving current vs. scanning angle

2.3 Reliability testing of mirror in water, continuous run

Following the characterization of the device, the next test was done to determine the device's operating lifetime at ±3° scanning angle in water. The experimental setup was the same as that used during characterization. The operating frequency was kept fixed at 183 Hz throughout the whole test and the driving current was adjusted to keep the scanning angle at ±3°. The mirror was kept underwater for the whole duration of this testing phase. The data recorded are presented below in Figure 2.7.

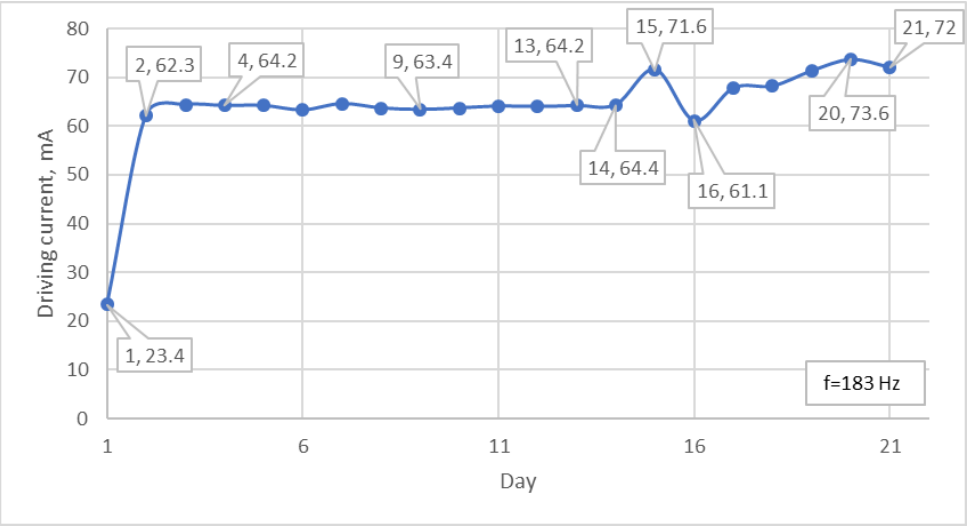

Figure 2.7 Reliability testing data in water, continuous run

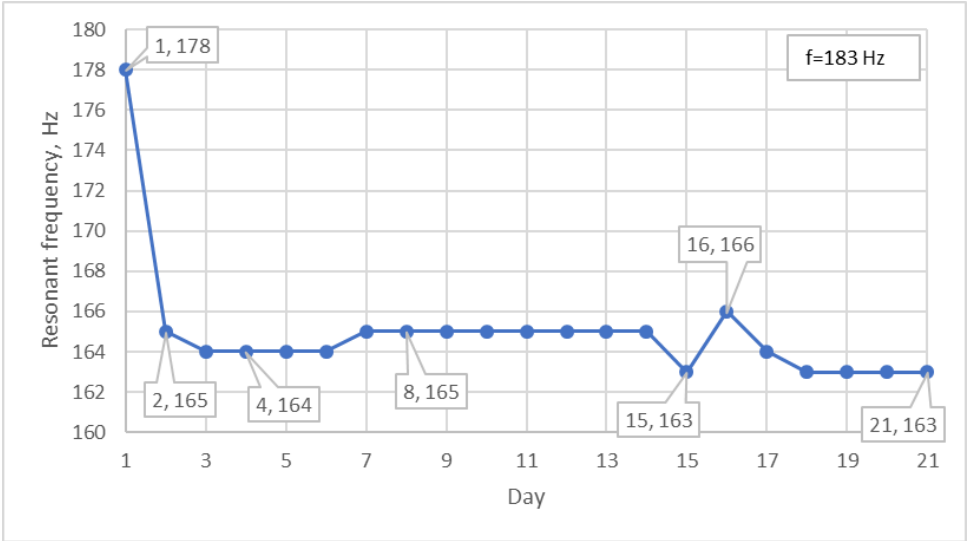

Figure 2.8 Reliability testing resonant frequency data in water, continuous run

The resonant frequency at the start of the test was 178 Hz and required current 23.4 mA. This increased to the 62.3 mA when measured on the second day, with the resonant frequency now being 166 Hz. Around here seems to be the normal region of operation,

with all subsequent current readings close to the 60-70 mA range and resonant frequency hovering around 165 Hz. With these results, it could be surmised that the polymer hinge structure needs to go through a process of ‘break-in’ at the start of operation to a more stable value. The shift in resonant frequency over the break-in process seem to be around 12-15 Hz in water, with an increase of around 40-50 mA in current required if operation frequency is kept unchanged. The lifetime of the device also exceeded expectations, with the device performing normally over 500 hours of continuous runtime. The test was stopped once the run exceeded 500 hours.

2.4 Reliability testing of mirror in water, cycles

The mirror was run in 8 hour cycles each day; this was to better simulate heavy but practical running conditions for the device in industry. The device was taken out of water at the end of a cycle and put back in the next day to do the following run. The data collected over 15 such cycles is presented in Figure 2.9.

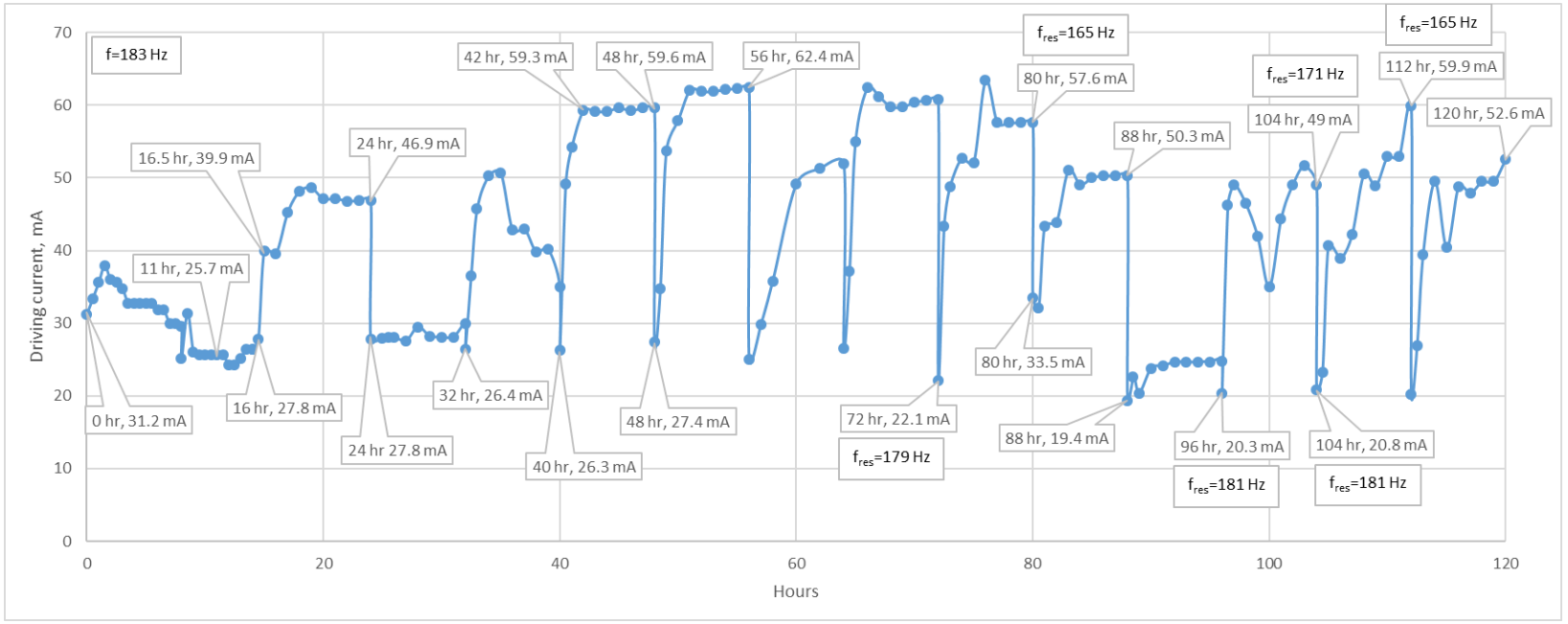

Figure 2.9 Reliability testing data, cycles

Starting from the first cycle (0-8 hours), it can be seen that the driving current required for ±3° was higher, 31.2 mA, than in the characterization test, 22 mA; however, it fell back down to around 25 mA in the second cycle (8-16 hours). It is from the third cycle (16-24 hours) that the break-in pattern began to emerge. A significant increase in driving current was required over the third cycle, with almost double the current was required by the end at 46.9 mA to keep the scanning angle at ±3°, compared to the start at 26.4 mA. This would normally indicate a degradation taking place in the device but, at the start of the next cycle (24-36 hours), it was observed that the driving current required for ±3° was 27.6 mA, similar to the measurement at the start of the previous cycle. This lead to the hypothesis that a form of temporary degradation and restoration might be taking place in the device's polymer hinge structure.

Looking at the data, it can be safely affirmed that there is no general discernable upward or downward trend in readings over the 120 hour test run. However, the required driving current does vary over a significant range of values within a run cycle. The required current can be close to 20 mA at the start of a cycle and increase threefold to 60 mA driving current required to maintain ±3° angle at the end. This change is also correlated to the change in resonant frequency of the device. The resonant frequency was also measured alongside the driving current over one of the test cycles, this data is presented in Figure 2.10. It can be observed that the required current increases in part of the resonant frequency shifting further and closer to the operating frequency of 183 Hz.

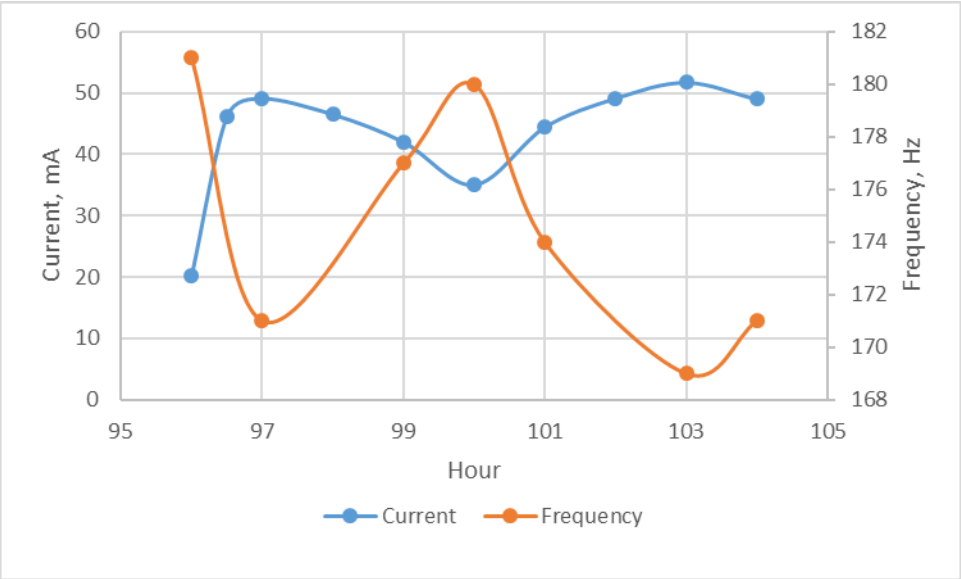

Figure 2.10 Resonant frequency vs. driving current shifts

The device seems to undergo a process of 'break-in' at the start of most cycles. The required current is always lower at the start and then gradually increases to a higher stable value which could possibly be considered the device's normal region of operation over a longer runtime cycle.

2.5 Reliability testing of mirror in air, cycles

The next reliability test the mirror underwent is for ±3° scanning angle with 8 hour run cycles in air. From this test, it was hoped to determine if the polymer structure behaved the same in air as in water. The resonant frequency in air for the mirror was determined to be 218 Hz during the characterization tests and that value was used as the driving signal frequency throughout this phase of the tests.

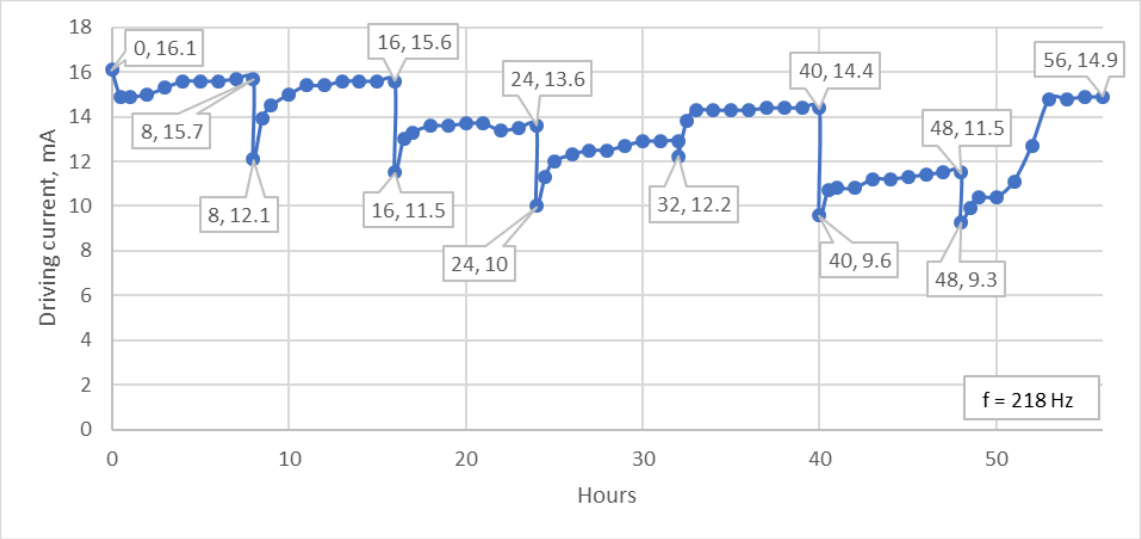

Figure 2.11 Reliability testing data in air, cycles

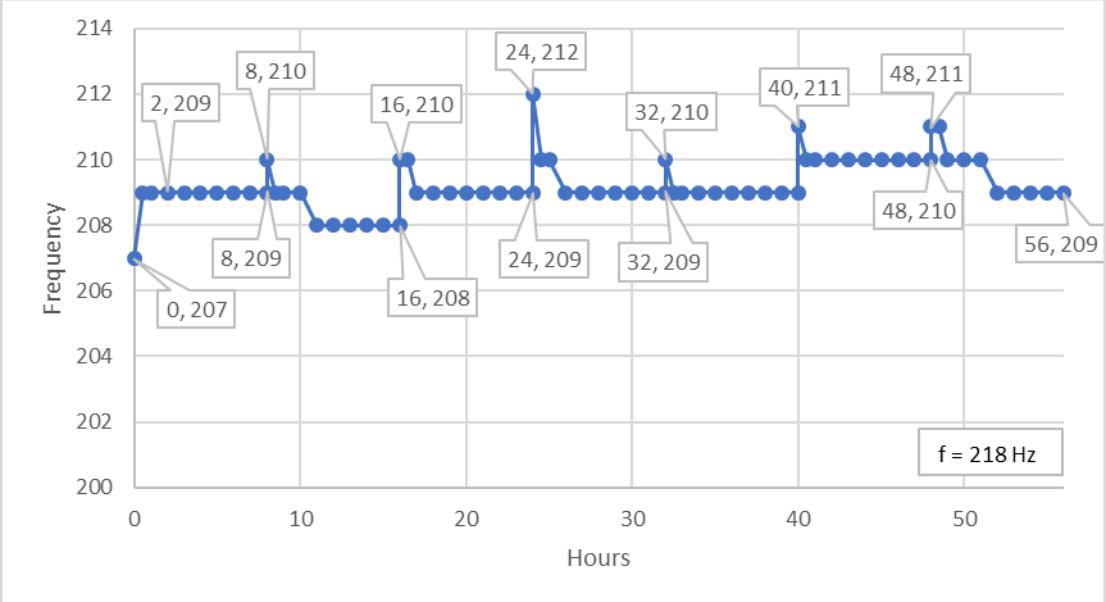

Figure 2.12 Reliability testing resonant frequency data in air, cycles

The data collected is presented in Figure 2.11, and it can be observed that the pattern of 'break-in' in between cycle are present here as well. From the first few cycles

the driving current values seemed to have been following a downward trend, but it did not continue to hold firmly past the fourth cycle, with current values going back up. The current values stayed within the 12-16 mA range, and resonant frequency staying within the 208-211 Hz range over this test. It could be concluded that the mirror operates similarly in both mediums at ±3° scanning angle.

2.6 Reliability testing of mirror in water, large angle, cycles

The next and final test performed on this version of our mirror device is ±6° scanning angle in water, with 8 hour operation cycles. The data collected is given in Figure 2.13.

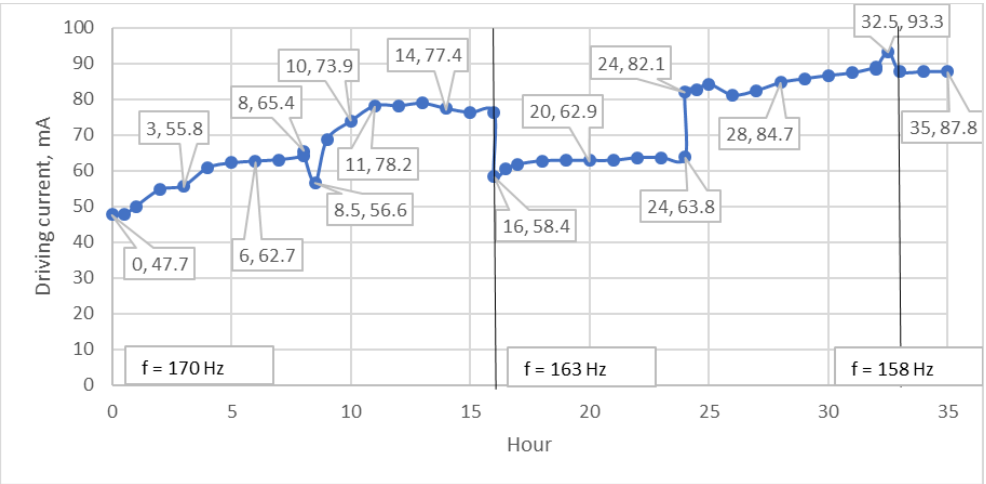

Figure 2.13 Reliability testing data in water, large angle, cycles

The signal frequency was tried to be kept at 183 Hz like the previous test, but the device quickly failed to register ±6° scanning angle within 10-15 minutes of operation with driving currents less than 100 mA, which is the maximum amount of current our

signal generator could output to the device. Hence, a new signal frequency was chosen at 170 Hz and proceeded forward with the testing.

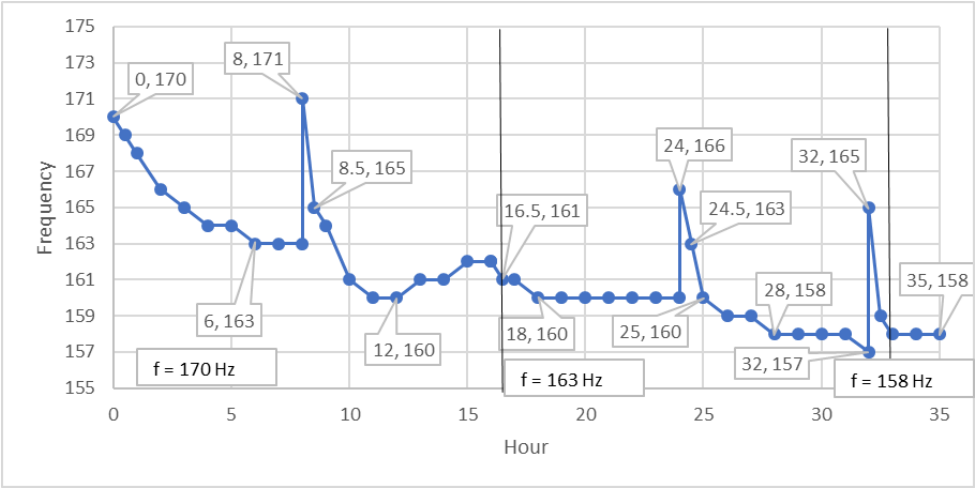

Figure 2.14 Reliability testing resonant frequency data, large angle, cycles

For the first two cycles of this test, it can be observed that an increasing trend in the required driving current is needed for ±6° angles, requiring 47.7 mA at the start of the first cycle and 77.4 mA at the end of the second. The resonant frequency also dropped from 170 Hz to 162 Hz. But during the third cycle, the device could no longer reach ±6° scanning angles at a signal frequency of 170 Hz, and it had to be decreased to match the new resonant frequency of the device at 161 Hz.

The third and fourth cycles showed the same trend in driving current increase, the third cycle needing an average of 62 mA and the fourth cycle needing 83 mA. Upon the start of the fifth cycle, the mirror could still reach ±6° at 161 Hz signal frequency with a required driving current of 93.3 mA; but an hour into this cycle, the signal frequency needed to be changed to 158 Hz as it could not reach ±6° under less than 100 mA current. The mirror managed to scan at ±6° angle for the next 2 hours at a driving current of 87.8

mA, but again failed to reach ±6° after. The signal frequency was again tried to be adjusted to make the mirror reach ±6° scanning angle, but this time it did not manage to reach the desired angle at any signal frequency with a driving current of less than 100 mA, at which point the test was stopped.

2.7 Conclusion

The mirror had a total operation runtime of 659 hours; 120 hours in the ±3° scanning angle in 8 hour cycles, 504 hours in the ±3° continuous run test, and 35 hours in the ±6° 8 hour cycle test. From the tests, it could be concluded that the single axis mirror using polymer hinge structure design is able to reliably operate at ±3° scanning angles and has a long lifetime more than satisfactory for use in the photoacoustic and ultrasound imaging industry. However, it could not hold up the same integrity in performance when operated at ±6° scanning angles, quickly deteriorating and unable to reach said scanning angle.

3. DESIGN AND FABRICATION OF NEW MIRROR DEVICE AND FURTHER RELIABILITY TESTING

3.1 Improvements to mirror device design and fabrication overview

In the previous chapter, the reliability of the polymer hinge structure based design water-immersible scanning mirrors was proven, given it operates under certain scanning angles and is not subject to shear strain enough to cause permanent degradation over time. The shear strain on the polymer hinges can be determined by,

$$\gamma = \frac{\emptyset\rho}{L}$$

where γ is the shear strain, $\emptyset$ is the scanning angle, ρ is cross-sectional area, L is the length of the hinges.

Doubling the scanning angle from ±3° to ±6° doubles the amount of shear strain, which the hinges cannot sustain without resulting in degradation. So, to keep the strain same at ±6° scanning angle, the length of the polymer hinges can be doubled .

Based on this theory, a new design for the polymer structure was created. The length of the hinges in this new design is double that of the previous one, and the outer shape has also been made into an ellipse to accommodate for an elliptical mirror plate that would reduce damping resistance in water. The computer-aided design (CAD) drawing of the previous and new polymer structure are given in the Figure 3.1.

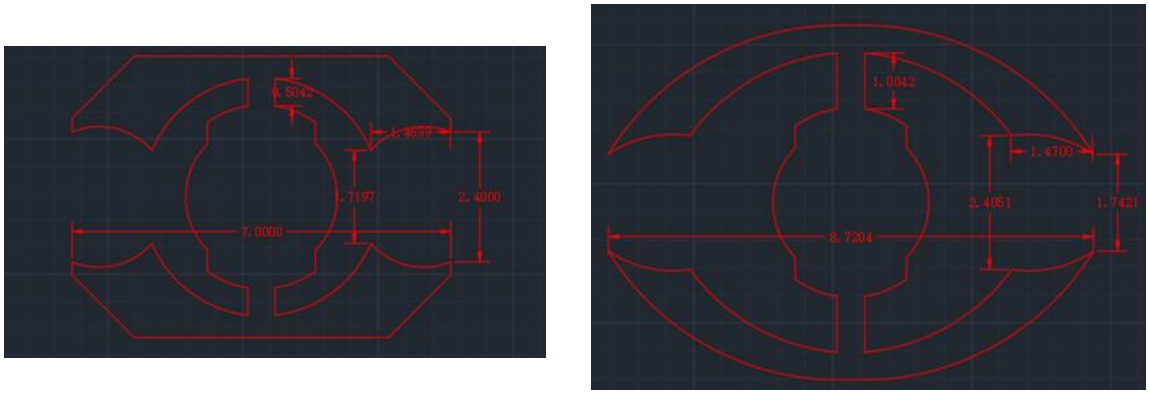

Figure 3.1 (a) Previous hinge design and (b) new hinge design

The length of the hinges in the previous design was 0.5 mm and has been doubled to 1 mm in the new design. An elliptical shape was also chosen over a circular one to allow for more incidence area to steer laser beams and ultrasound waves.

Corresponding elliptical acrylic spacers were also designed to accompany the new hinge structure. The designs were then cut using a laser cutting machine (PLS6.75, Universal Laser System) with the polymer hinges cut out from 75 µm thick BOPET film, and the acrylic spacers cut from 1mm thick acrylic sheet. The new mirror was assembled with the redesigned elliptical spacer and hinge replacing the previous ones, but the rectangular mirror plate was left as is for now. The purpose of assembling this mirror was to test out the new hinge structure, and to verify first if it could solve the reliability issue at ±6° scanning angles.

3.2 Characterization and testing of new mirror device

The mirror was characterized at ±6° first in the same process as before and the values recorded are provided in Table 1.

	Resonant frequency	Driving current
Air	126 Hz	26 mA
Water	90 Hz	62 mA

Table 1 Characterization results of new mirror device

The mirror's operation was then tested in water with 8 hour run cycles and the data collected is presented in Figure 3.2.

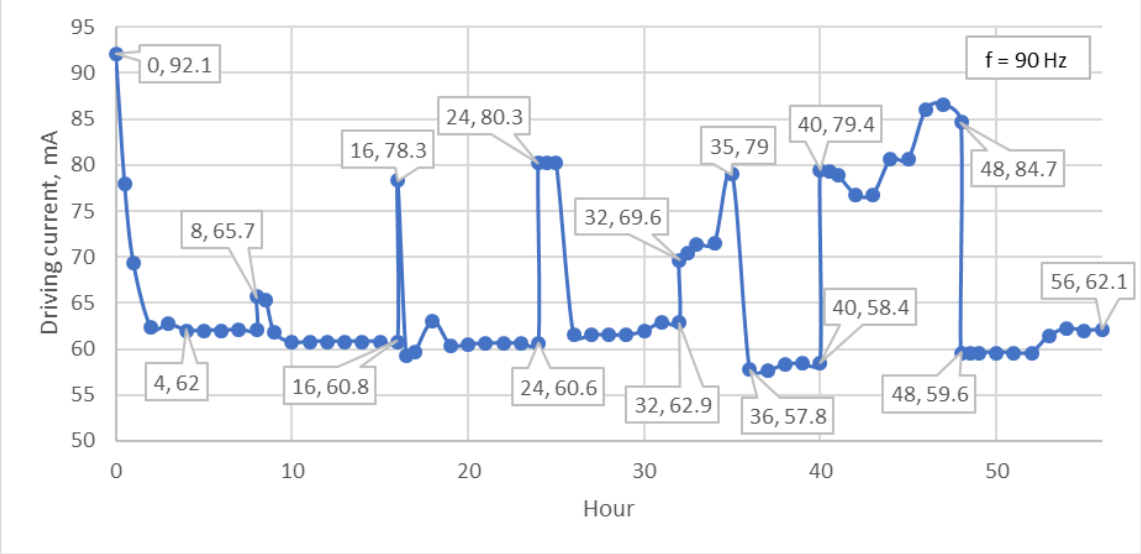

Figure 3.2 Test data in water, new device

The signal frequency was kept fixed at 90 Hz, and the current is adjusted to keep the scanning angle at ±6°. The mirror started off requiring 92.1 mA of current but quickly dropped to the 62 mA probably following the 'break-in' process. This pattern repeats for all the 4 cycles totaling a run time of 32 hours. The resonant frequency of the device stayed constant at 90 Hz throughout the whole run. No deterioration in the performance could be observed from these experimental results as was present with the previous polymer hinge.

3.3 Fabrication of elliptical mirror plate

The change in design of the hinge seemed to have resolved the issue of degradation at ±6° scanning, but the resonant frequency had dropped considerably from 183 Hz to 90 Hz. Our next objective was to bring up the resonant frequency so that the device could be operated satisfactorily at 100 Hz signal frequency. We hence moved on to fabricate the elliptical mirror plate to replace the current rectangular one, which would result in reduced damping resistance experienced by the device in water, as well as slightly cut down the weight of the mirror plate and bring the resonant frequency up.

To fabricate the new mirror plate, reactive ion etch (RIE) was used to etch out the plates out of an aluminum deposited single-crystal silicon substrate. The photomask layout was created using L-Edit and is given in Figure 3.5. The dimensions of the ellipses are 8.73 mm along the major axis and 6.38 mm along the minor axis.

After the photomask was created, the substrate on which the mirrors would be etched was readied. Using an electron beam evaporator (PVD 75 Ebeam Evaporator, Lesker), a 150 nm layer of aluminum was deposited on to a 2-inch single-crystal silicon

wafer. Following the deposition, the photomask pattern was transferred on to our wafer using photolithography and an aluminum etch. Following this, we used RIE (Plasmalab 100 RIE System, Oxford Instruments) to etch away the surrounding silicon and leave us with just our aluminum deposited elliptical silicon mirror plates.

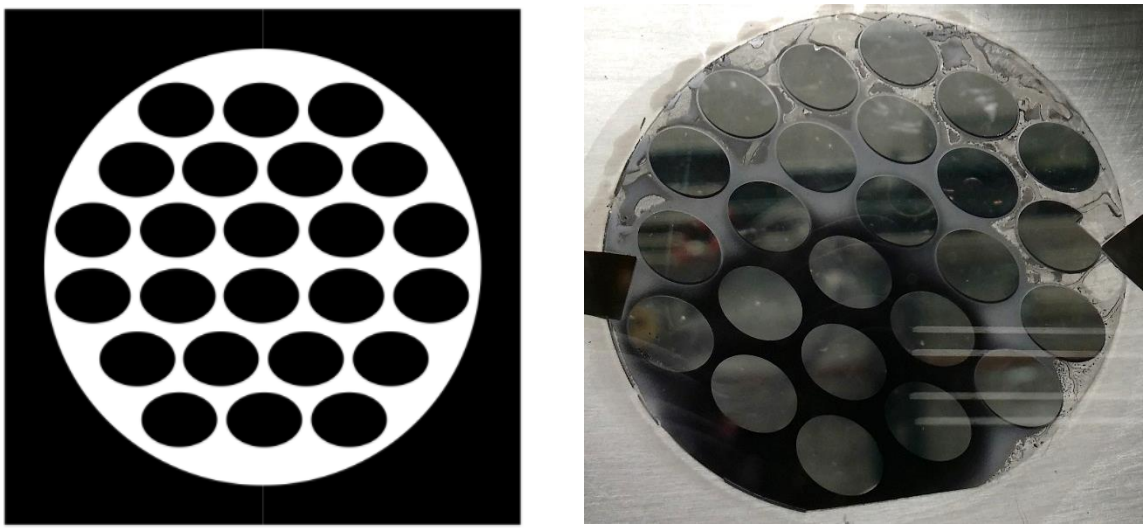

Figure 3.3 (a) Photomask layout for elliptical mirrors and (b) etched out mirror plates

3.4 Characterization and reliability testing of new device with elliptical mirror plate

A new mirror was then assembled trading in the rectangular mirror plate for the elliptical one and then characterized. The 3D model of the new mirror is given in Figure 3.4 and the characterization results are provided in Table 2.

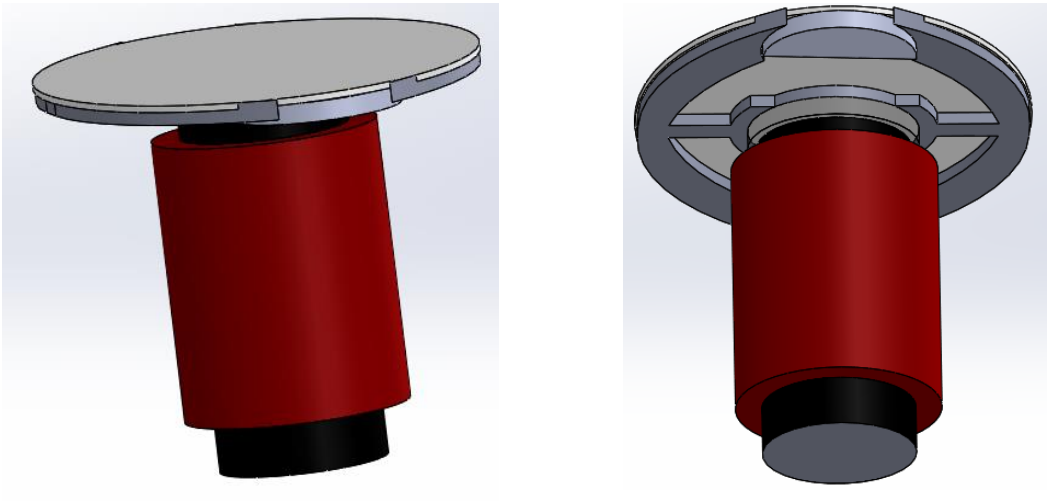

Figure 3.4 3D Model of new mirror

	Resonant frequency	Driving current
Air	125 Hz	16.3 mA
Water	100 Hz	65.1 mA

Table 2 Characterization results of new mirror device with elliptical mirror plate

The resonant frequency with the new mirror plate remained around same in air, but an increase of 10 Hz was seen under water, from 90 Hz recorded in the previous mirror to 100 Hz. With the bump in resonant frequency achieved as expected, the next phase of the reliability testing of this mirror was proceeded to.

The mirror was tested for ±6° scanning angle in water medium, with the signal frequency set at 100 Hz matching the resonant frequency characterization result. The mirror was run in 8 hour cycles per day, with the mirror taken out to dry between cycles. The data collected over 17 cycles of tests done on the mirror are presented in Figure 3.5.

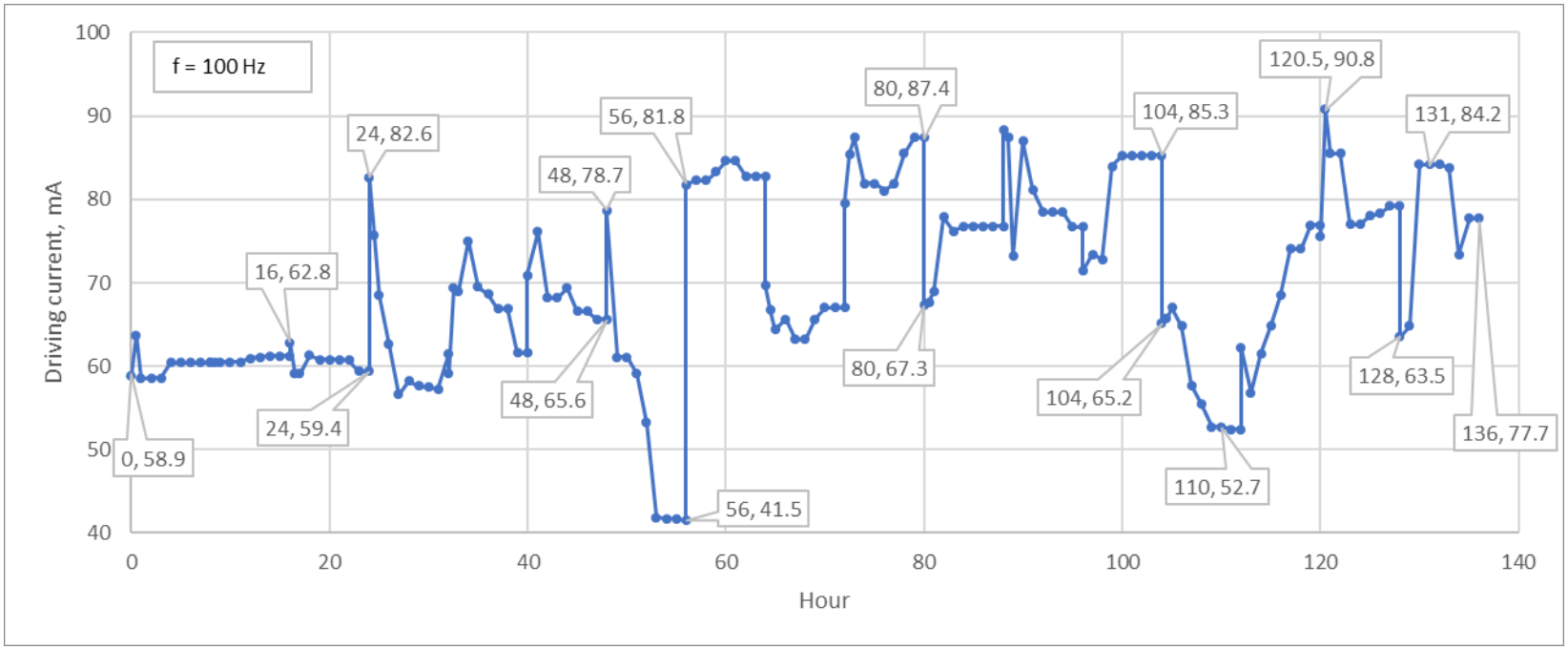

Figure 3.5 Reliability test data in water, new device

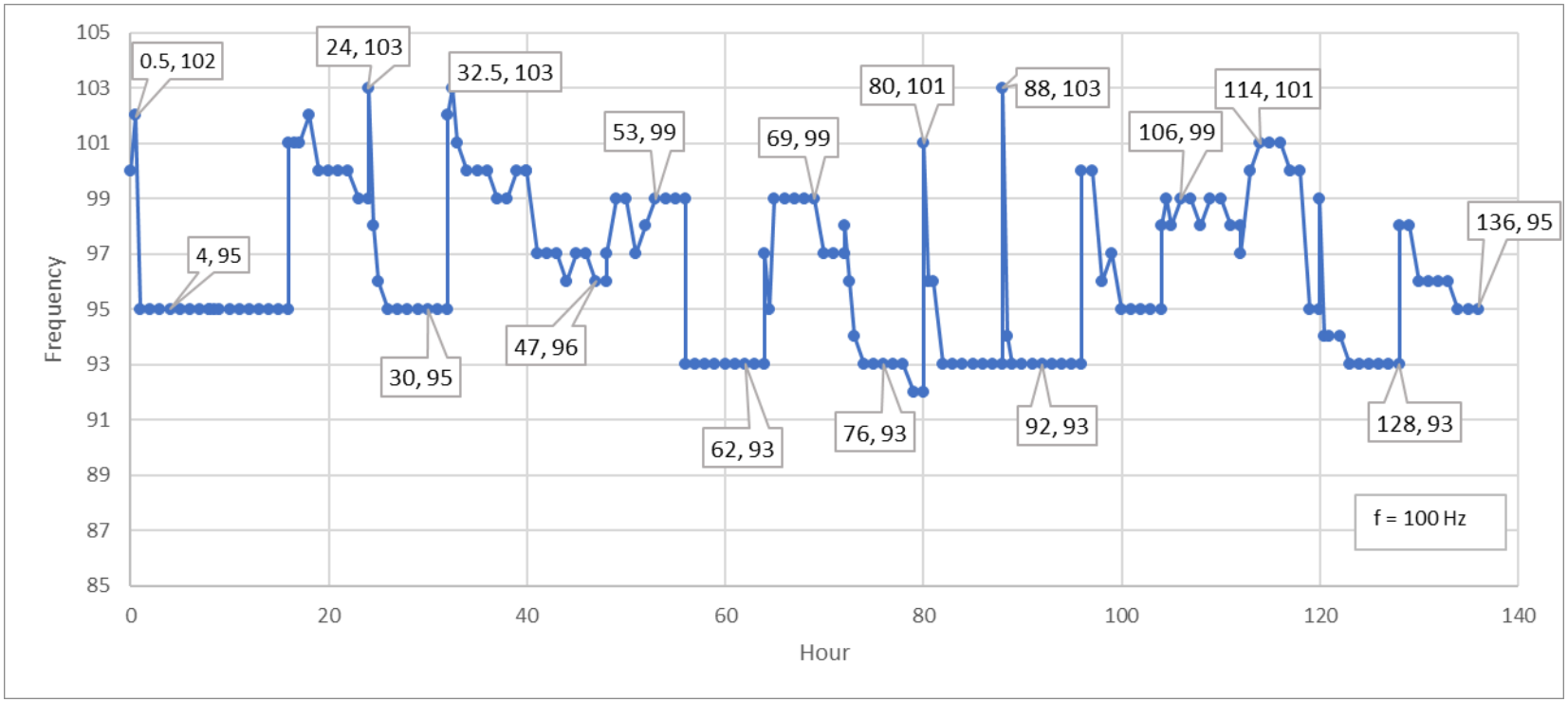

Figure 3.6 Reliability test resonant frequency data in water, new device

From the current value plot, a similarity could be observed between the data for this mirror running at ±6° and the first mirror design tested at ±3° scanning angles. The driving current required varies over a wide range here as well from the lowest recorded at 41.9 mA to the highest at 90.8 mA, but no decipherable up or downtrend could be observed in the values, meaning no degradation occurred in the device. The resonant frequency varied between 93-103 Hz, but the device could be always be operated at reasonable driving currents at 100 Hz signal frequency, which was the aim for the elliptical mirror plate based design.

3.5 Conclusion

Following the identification of the reliability issue faced by the original mirror at ±6°, modifications were made to the polymer hinge structure, doubling the hinge lengths to acquire double scanning angle at the same torque as ±3°. The shape of the hinges was also made elliptical to accommodate for an elliptical mirror plate fabricated using RIE. The new device managed to operate reliably at our desired ±6° scanning angle in water with no sign of degradation over the 136 hour testing run.

4. IMPLEMENTATION OF SCANNING ANGLE MEASUREMENT SYSTEM

4.1 Introduction

There are many forms of magnetic sensing technologies used throughout applications in research and industry. From inductive coil magnetometers to MEMS based magnetic sensors, each has its own set of pros and cons when it comes to size, sensitivity, sensing range and costs. But the most readily available and cost-effective commercial magnetic sensors utilize the Hall effect phenomenon to measure magnetic fields.

From the reliability test data collected from our mirror device, though it could be concluded that the new design was able to run at ±6° without degradation in performance, the driving current did need to be adjusted to maintain the angle at a fixed value. To further the reliability of the device in the sense of keeping the angle stable, the angle of the device must first be able to be read accurately and continuously. This chapter details the process of implementing magnetic sensing using a Hall sensor to precisely monitor the scanning angle and then its subsequent addition to the device package.

4.2 Magnetic field simulation and Hall sensor specifications

First, the magnetic field of the device configuration is simulated in order to find the magnitude of the field and the ranges of concern so as to properly select a Hall effect sensor to fit the device's needs. The simulation was done using FEMM and the results are shown in Figure 4.1.

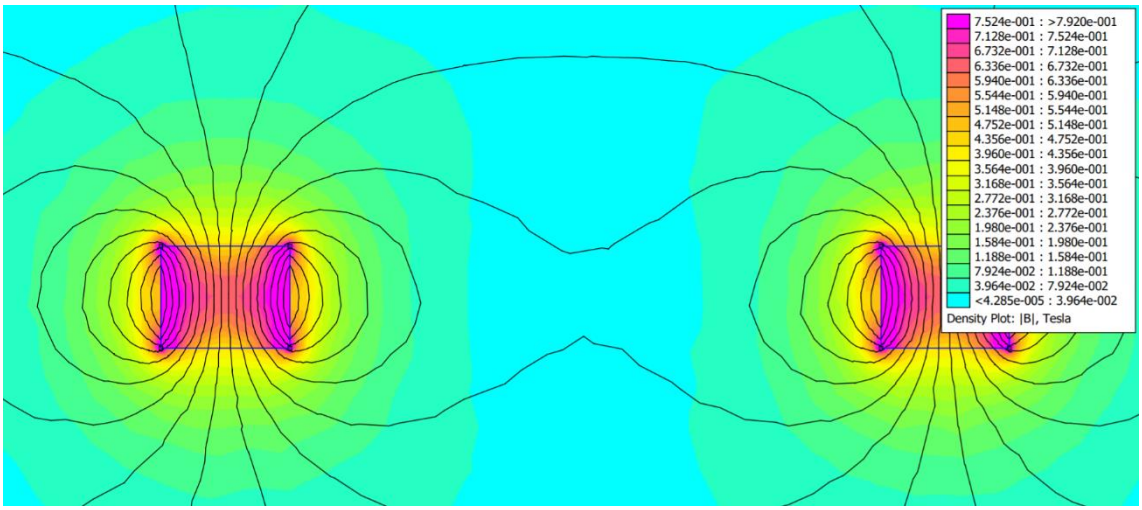

Figure 4.1 FEMM simulation of device configuration permanent magnets

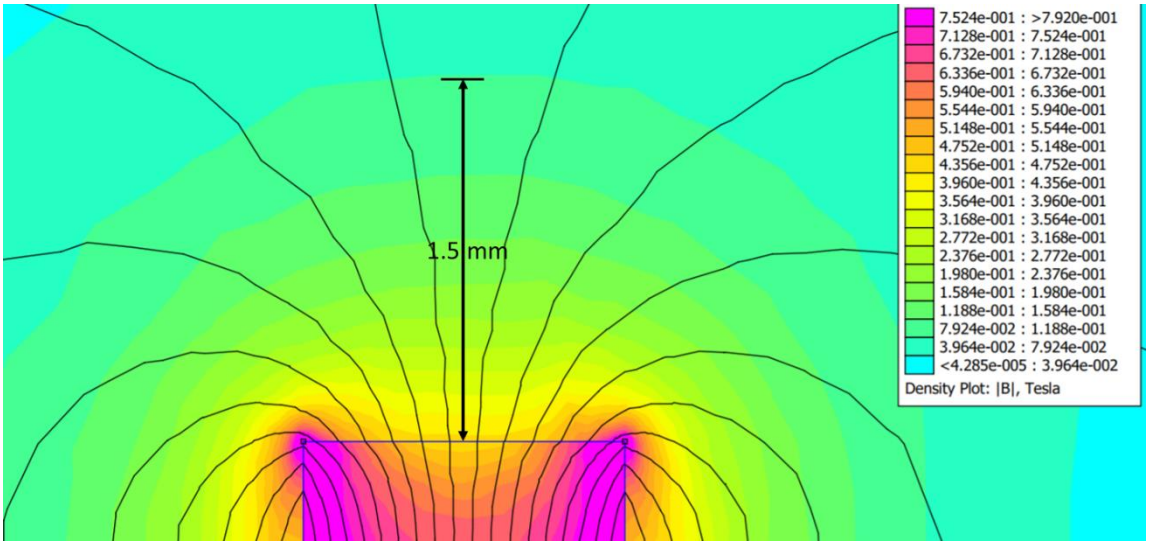

Figure 4.2 Region of interest for Hall sensor placement

Two NdFeB Grade 40 magnets were placed 7.25 mm away with opposite polarity directions, and the strongest field reading could be seen to be around 400 mT at the top surface along the center. At 1.5 mm away from the top, the field can be seen to range in

between 40 mT to 80 mT. This is a reasonable length of distance to place the sensor at so to not accidentally come into contact with the mirror during scanning. Based on this, the analog linear Hall-effect sensor SS49E from Honeywell was chosen. It operates within this magnetic field range and has a package size of 4.1 mm x 1.6 mm x 3 mm, close to the range of our mirror device's dimensions. Having a linear response also will allow for easier calibration of the Hall sensor reading to our mirror's scanning angle. The specifications of the Hall sensor are given in Figure 4.3.

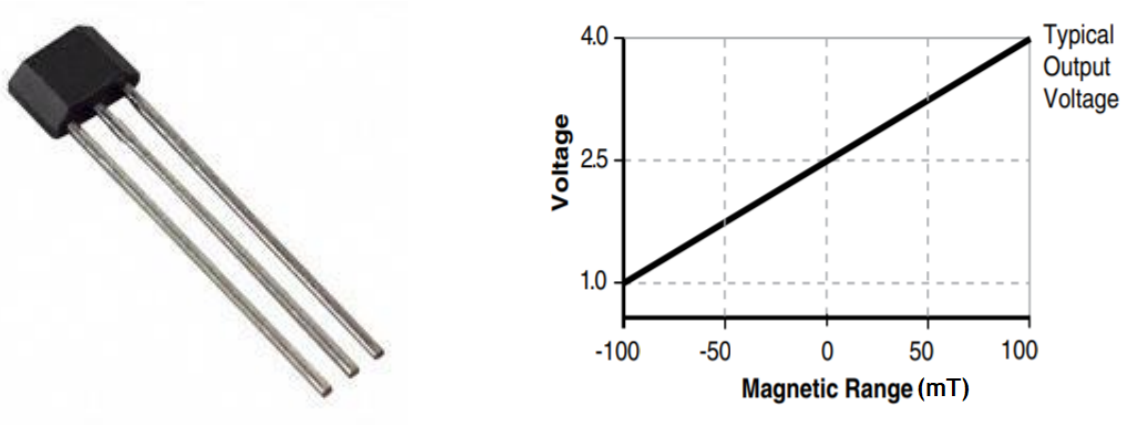

Figure 4.3 (a) Honeywell SS49E Hall sensor and (b) its response provided in specification sheet

4.3 Hall sensor characterization

After receiving the Hall sensor, the device was first characterized. The output voltage of the Hall sensor was measured against its separation from a fixed permanent magnet, with the help of a linear translational stage (M403.2DG Precision Translation Stage, Physik Intsrumente). The Hall sensor was held in place at the fixed end of the stage, and the permanent magnet moved away from the sensor in steps whilst recording the Hall

sensor output voltage. The setup schematic is shown in Figure 4.4. The output voltage against separation plot is given in Figure 4.5 as well as the corresponding sensitivity in Figure 4.6.

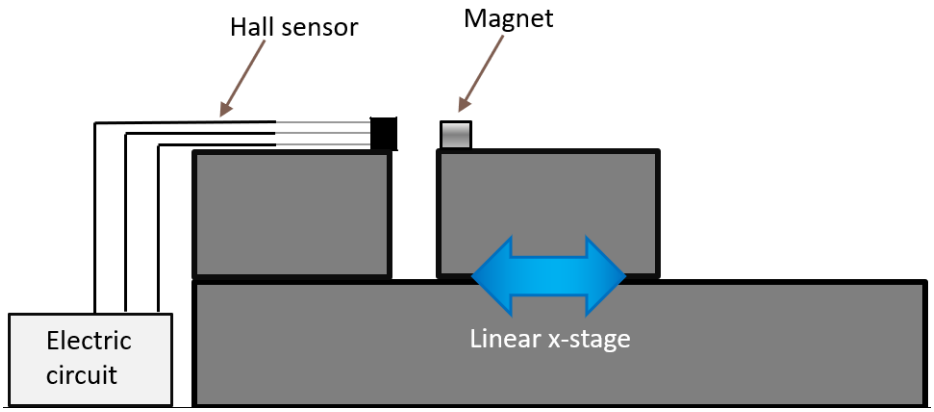

Figure 4.4 Experimental setup for Hall sensor characterization

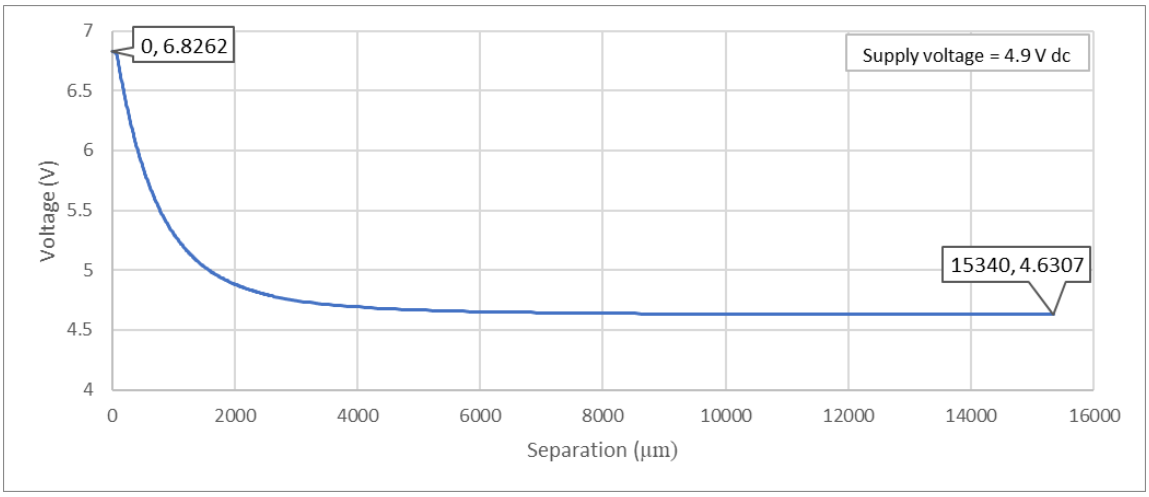

Figure 4.5 Hall sensor characterization, output voltage vs. separation

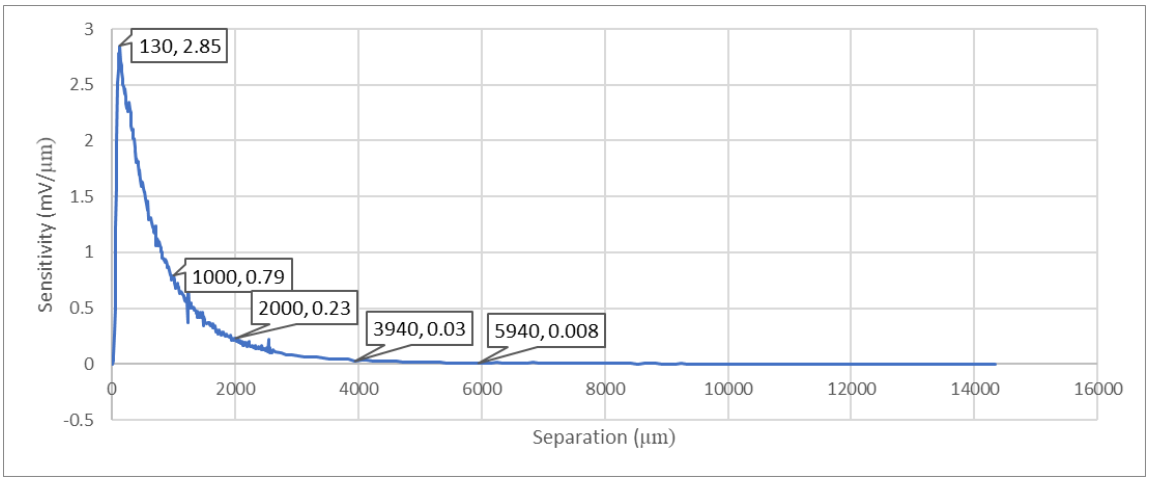

Figure 4.6 Hall sensor characterization, sensitivity vs. separation

From the plots, it could be seen that the relationship in both cases is an inverse exponential versus the separation due to the magnetic field cutting the Hall sensor area decreasing in the same rate. The translation the mirror plate goes through is approximately 76 μm per 1° scanning angle, so since the objective was to keep the scanning angle fixed at ±3° or ±6°, the device would be working inside a linear region of the sensitivity curve making calibration simpler.

4.4 3D printing of new holder and device assembly

Since the Hall sensor had been characterized and shown to meet the specifications for scanning angle monitoring, it was then proceeded to be incorporated into our device package. The previous 3D printed holder's design was modified to accommodate for the Hall sensor, by adding an elevated extension to serve as a base for the Hall sensor to be

put on to. The model of the new holder is given in Figure 4.3. The holder was 3D printed with photopolymer resin using an optical 3D printer (Nobel Superfine, XYZPrinting).

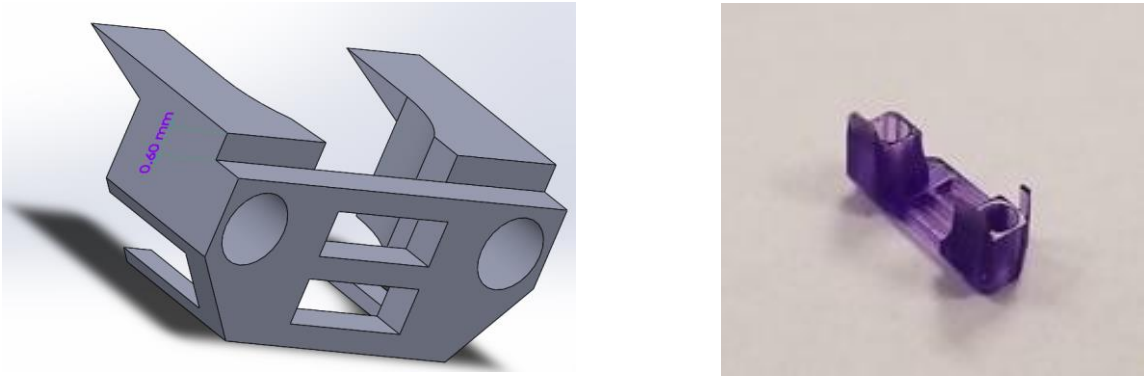

Figure 4.7 (a) 3D Model of new holder and (b) 3D printed new holder

For the next step, in order to place the Hall sensor properly on the new holder and below the magnet, the Hall sensor was sanded, reducing its thickness down from 1.6 mm to 0.8 mm using a file. This allowed the Hall sensor to be placed properly with enough space provided for the mirror's motion whilst being close enough to the magnet to ensure good sensitivity. The Hall sensor was glued to the extension of the holder using silicon adhesive (RTV 108, Momentive Performance Materials).

Figure 4.8 (a) Assembled device package and (b) top view

4.5 Calibration and testing of Hall sensor scanning angle monitoring

Following the construction of the mirror device with the Hall sensor, it was then calibrated and tested to see how accurately the scanning angle could be measured. The experiment was done in air medium with the setup being as before in all the reliability tests. The Hall sensor output was connected to a digital oscilloscope (TDS 2014B Digital Storage Oscilloscope, Tektronix) from which the peak-to-peak amplitude of the oscillating output voltage of the Hall sensor could be measured by the oscilloscope. The average function of the oscilloscope was also used to remove noise, which averaged 64 sequences of waveforms and display the computed waveform.

The peak-to-peak voltages were first calibrated to corresponding scanning angles of the device, determined by using the laser tracing method as in previous tests. The scanning angle was decreased in 0.1° steps starting from 3° up to 1°, and the corresponding

peak-to-peak voltage values recorded. It was then again brought back up to 3° angle in 0.1° steps to test for repeatability in the peak-to-peak values registered, and the same amplitudes were recorded. This was repeated two more times, and peak-to-peak voltages values recorded remained same through all three repetitions. The plot of the data collected is given in Figure 4.9.

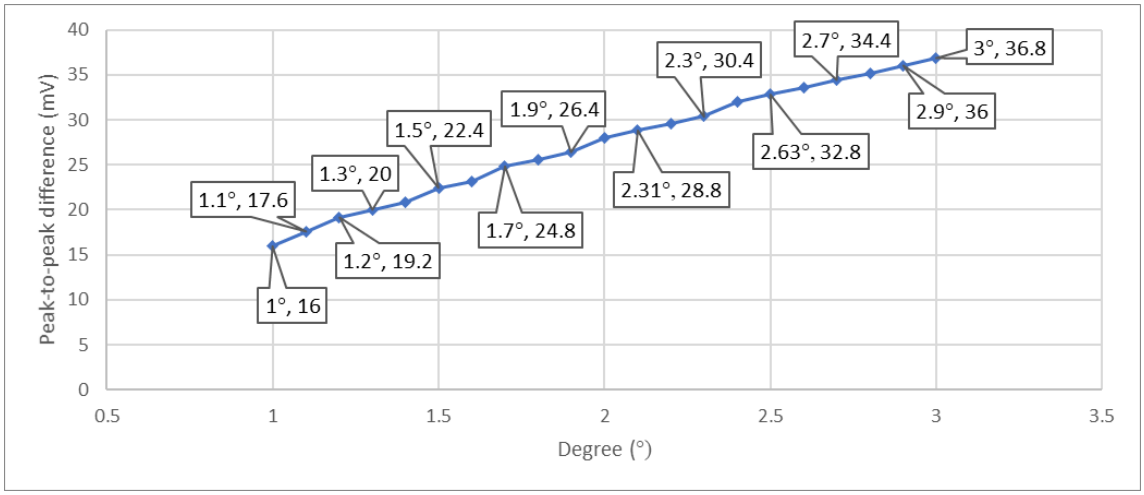

Figure 4.9 Hall sensor data from angle monitoring calibration and test

The relationship between the scanning angle and Hall sensor output can be seen to be linear from the plot, with around 0.1 mV change in output voltage measured for each 0.1° change. The sensitivity obtained, though less than expected in theory, is still good enough to be able to monitor our scanning angle with the desired precision.

4.6 Conclusion

In order to further increase the reliability of the mirror device's operation, a scanning angle monitoring feature using a linear Hall effect magnetic sensor was introduced. The range of magnetic field strength that our device's permanent magnet

configuration produced was first determined through simulation. Based on the results, a suitable linear analog Hall-effect sensor was chosen.

Sensor characterization was done to obtain the response of its output voltage to distance from a permanent magnet, from which the sensor's linear response in the region of interest was determined. To then accommodate the sensor in the device, the 3D printed holder's design was changed to be able to hold the Hall sensor below the magnet, and the sensor was also sanded to reduce its thickness by half before adding it to the device package.

Following this sensor's output was then calibrated to the corresponding scanning angle, after which the repeatability of the output voltage measured versus scanning angle was tested. It was shown to be perfectly repeatable over three sweeps, and the sensor sensitive enough to be able to determine scanning angle up to 0.1° in precision.

5. CONCLUSION AND FUTURE WORKS

MEMS scanning mirrors have significant potential in applications of ultrasound and photoacoustic microscopy, providing a cost-effective, small form-factor solution to beam steering and scanning. Conventional silicon-based MEMS mirrors do not operate well in the required liquid medium needed for ultrasound, hence polymer-based designs were developed to resolve the issue. However, not much research has been done into determining the reliability of polymer material in such applications, which was the inspiration and aim of the study done in this thesis.

Extensive testing was performed on such a single-axis polymer hinge-based MEMS scanning mirror, in two different mediums of air and water, and at two different scanning angles of ±3° and ±6°. Through the tests it was shown that the mirror could operate reliably in both air and water at ±3° scanning angle. A 'break-in' phenomenon was observed to be taking place at the start of a test run, with shifts in the device's resonant frequency recorded and driving current needing to be adjusted to maintain the desired scanning angle. Though this was a pattern, there was no general deterioration seen over time in the performance of the device. But, a clear degradation in performance was seen when operated at ±6°, and the device quickly failed to reach the desired angle following a few test cycles. It was hence concluded that the polymer hinges were reliable given that the torque exerted on them did not exceed a certain limit, which if it did, resulted in permanent deformation occurring slowly over operation.

Based on the results of the tests, changes were made to the polymer hinge structure, doubling the length of the hinges to allow for double the scanning angle at the same torque. An elliptical shape was also implemented to lessen damping resistance experienced by the device operating in water. Following laser-cutting of the new hinge structure and fabrication of the elliptical mirror plates using RIE, the new mirror device design was assembled and tested. It was shown to operate reliably at ±6°, solving the reliability issue at that angle, and though a decrease in resonant frequency of the device was observed, it could still be operated at 100 Hz signal frequency which is satisfactory enough for scanning purposes.

To mitigate the effects of 'break-in' and required adjustments in driving current over a run cycle, a way to precisely monitor the scanning angle is required. Therefore magnetic sensing was implemented using a linear Hall-effect sensor added to the device package. The Hall sensor was chosen based on magnetic simulation results of the device permanent magnets, and then was characterized to determine sensitivity and response of the sensor. Following that, a new holder was designed that allowed the Hall sensor to be placed below the magnet of our mirror device and then was tested to determine the accuracy of the sensor readings. Following calibration, the sensor readings were shown to be correctly identify the scanning angle of the device, and highly accurate in its measurements. Precision of up to 0.1° monitoring of the angle was achieved.

For future works, this monitoring system could be utilized to create a feedback control system using microcontrollers and maintain a fixed scanning angle through automatic adjustments of driving current. The structural integrity and lifetime of the

polymer hinge-based design scanning mirrors was proven to be more than satisfactory in this study, and upon implementation of a feedback system in the future, the reliability of the device can be even more improved for use in applications in and beyond ultrasound and photoacoustic microscopy.

REFERENCES

1. M. H. Xu and L. V. Wang, “Photoacoustic imaging in biomedicine” Rev. Sci. Instrum., vol. 77, no. 4, pp. 041101, 2006
2. C. Zhang, K. Maslov, J. Yao and L. V. Wang, “In vivo photoacoustic microscopy with 7.6-μm axial resolution using a commercial 125-MHz ultrasonic transducer,” J. Biomed. Opt., vol. 17, no. 11, pp. 116016, 2012
3. S. Xu, C.-H. Huang and J. Zou. “Microfabricated water-immersible scanning mirror with a small form factor for handheld ultrasound and photoacoustic microscopy.” J. Micro. Nanolithogr. MEMS MOEMS, vol. 14, no. 3, pp. 035004, 2015
4. C.-H. Huang and J. Zou, “A novel two-axis micromechanical scanning transducer using water-immersible electromagnetic actuators for handheld 3D ultrasound imaging,” Sens. Actuators, A, vol. 236, no. 12, pp. 281-288, 2015